Near-field scattered by a single nanoslit in a metal film

Lionel Aigouy,[1,*] Philippe Lalanne,[2] Haitao Liu,[2,3] Gwénaelle Julié,[4] Véronique Mathet,[4] and Michel Mortier[5]

[1]Laboratoire Photons Et Matière, UPR CNRS A0005, Ecole Supérieure de Physique et de Chimie Industrielles (ESPCI), 10 rue Vauquelin, 75231 Paris Cedex 5, France

[2]Laboratoire Charles Fabry de l'Institut d'Optique, University Paris-Sud, CNRS, Campus Polytechnique, RD 128, 91127 Palaiseau cedex, France

[3]Key Laboratory of Opto-Electronic Information Science and Technology, Ministry of Education, Institute of Modern Optics, Nankai University, Tianjin 300071, China

[4]Institut d'Electronique Fondamentale, UMR CNRS 8622, Bâtiment 220/221, Université Paris-Sud, 91405 Orsay Cedex, France

[5]Laboratoire de Chimie de la Matière Condensée de Paris, UMR CNRS 7574, Ecole Nationale Supérieure de Chimie de Paris (ENSCP), Rue Pierre et marie Curie, 75231 Paris Cedex 5, France

*Corresponding author: aigouy@optique.espci.fr

Received 27 August 2007; accepted 22 October 2007;
posted 1 November 2007 (Doc. ID 86922); published 13 December 2007

Using a scanning near-field optical microscope, we visualize, in three dimensions, the electromagnetic field distribution near an isolated slit aperture in a thin gold film. At the metal-air interface and for a TM incident polarization, we confirm some recently observed results and show that the slit generates two kinds of surface waves: a slowly decaying surface plasmon polariton and a quasi-cylindrical wave that decreases more rapidly when moving away from the slit. These waves are not generated for a TE incident polarization. In a noncontact mode, we also observe how the transmitted light diverges in free space. At a small distance from the slit (< 2 μm), we find that the emerging light spreads in all directions for TM, forming an electromagnetic cloud, whereas it is concentrated above the slit for TE, forming a more directive light jet. The experimental images are in good agreement with the numerical simulations.

OCIS codes: 240.6680, 050.1220.

Light scattering by nanoapertures in thin noble metal films has recently been widely studied by scanning near-field optical microscopy (SNOM) and other unconventional techniques [1–5]. The interest in such a microscopic characterization is motivated by understanding the physics hidden behind the surface waves generation, their propagation, and their interaction with the local environment [6], but also by the design of new photonic and plasmonic devices or sensors [7,8]. Since the usually observed effects depend on many geometrical parameters of the apertures, such as their shape, their size, and their relative distance, the comprehension of basic phenomena can be eased by studying elementary structures, such as nanoholes or nanoslits, isolated on the metal surface or simply coupled two by two to minimize the number of varying parameters.

In this paper, we perform a study of the near-field distribution around an isolated nanoslit aperture as a function of the incident polarization direction. We will confirm some recently observed results that showed that the surface waves generated by nanoslit apertures in a metal film are the sum of two kinds of wave: a surface plasmon polariton (SPP) and another nonplasmonic quasi-cylindrical wave that decays at a much faster rate [4,9–11]. In contrast with previous near- and far-field measurements, the waves are directly visualized, without involving any multiple interference phenomena with the light transmitted through the substrate [1,3], with another SPP [2,4] or by far-field interferometry [10–12]. By performing scans in a noncontact mode in a plane perpendicular

0003-6935/07/368573-05$15.00/0

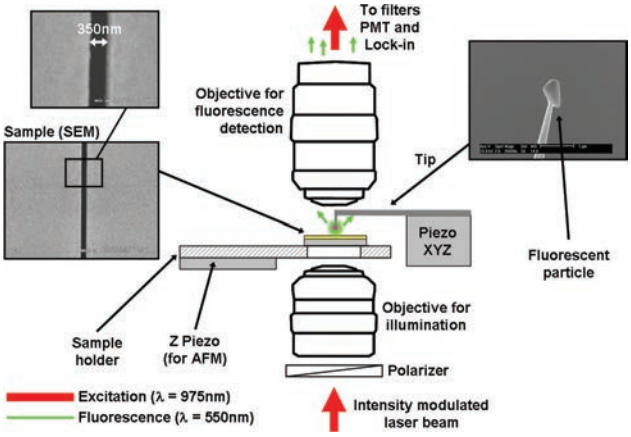

Fig. 1. (Color online) Experimental setup. Excitation is performed at $\lambda = 975$ nm and fluorescence is recorded at $\lambda = 550$ nm.

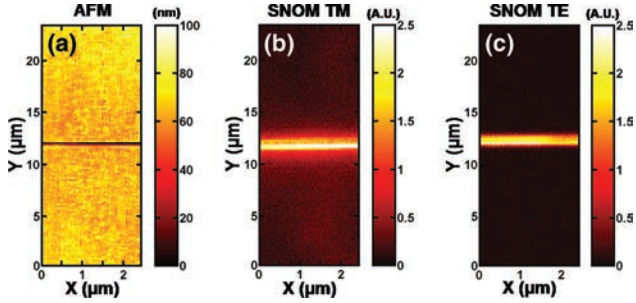

Fig. 2. (Color online) (a) Topography and (b) SNOM images for TM, and (c) TE incident polarizations. The "background" observed on the whole TM image is due to surface waves launched on the metallic interface.

to the surface and to the slit axis, we have also been able to observe how the light diverges in the far-field for both polarizations. At a short distance from the aperture (< 2 μm), the light emerging from the slit spreads in all directions for TM forming an electromagnetic cloud, whereas it is much more directional for TE forming a narrow beam above the slit.

The sample consists of a slit aperture (width $= 350$ nm, length $= 20$ μm) made in a 100 nm thick gold film on a fused silica substrate by electron-beam lithography and subsequent ion-beam etching. A 5 nm thick chromium layer was sputtered on the glass prior to the gold deposition to ensure good adhesion. A scanning electron microscope image (SEM) of the structure is shown in Fig. 1, with a sketch of the experimental setup. The SNOM apparatus used in this study is different from the configurations usually employed in near-field optics (see, for instance, [1–3] and [13–15]). It uses a fluorescent particle glued at the end of an atomic force microscope tip to detect the local electromagnetic field [16]. Although unusual, the fluorescence of films deposited on metal surfaces has recently been employed by several groups to detect surface plasmon fields with far-field microscopy techniques [17,18]. In the present case, the fluorescent material has a subwavelength size (~300 nm), providing a lateral resolution in the order of $\lambda/3$. It is made of an erbium/ytterbium codoped fluoride glass, highly fluorescent, and chemically stable. The compound is excited in the near-infrared ($\lambda = 975$ nm) and the fluorescence that involves a nonlinear absorption process called up-conversion is collected in the visible range (530–550 nm). Under such excitation, we therefore expect to detect the square of the electromagnetic field intensity. Besides, since the material structure is amorphous, the probe is sensitive to all components of the electromagnetic field, giving a representation of the total electric field on the surface. Under direct illumination by a laser beam, the particles can emit up to 10^6–10^7 photons per s, offering a good signal-to-noise ratio. For the experiments, the tip is scanned above the sample with an *XYZ* piezoelectric stage, and both the sample and illumination remain static. The tip is movable in all three directions allowing scans to be performed either on the surface (*XY* mode) or in planes perpendicular to the sample (*XZ* or *YZ* modes). For a *XY*-type scan, the tip/sample distance is maintained constant in the tapping mode (oscillation amplitude ~10–20 nm) with a feedback loop. For the *XZ*- or *YZ*-type scans, the feedback loop is disabled and the tip freely moves above the sample. The latter is illuminated from the rear side by a 975 nm laser diode polarized in a direction either parallel (TE) or perpendicular (TM) to the slit axis. The incident beam is only weakly focused, so that the entire slit is illuminated.

The recorded topography and the SNOM images of the nanoslit structure are given in Fig. 2. The light transmitted through the slit is apparent, both for TE and TM polarizations. However, in the TM case, an additional electromagnetic field background is clearly visible on the whole image. As will be shown hereafter, it corresponds to surface waves launched by the aperture on the metal-dielectric interface. To characterize this surface field, we have averaged the optical images of Fig. 2. The averaged cross-section data over all the columns of the images are displayed in Fig. 3. We clearly observe that the surface waves are generated only for TM polarization. Indeed, the only direction of the incident electromagnetic field that can efficiently create charge oscillations associated to surface waves on both sides of the slit is TM. This is consistent with previous theoretical simulations [19], far-field transmission measurements [12], and near-field observations on nanoholes [1] or ring apertures [2], which all show that the SPPs are launched in the direction of the incident polarization. We note that the surface wave generation is not symmetric on both sides of the slit. This difference can be explained by the fact that the laser beam may impinge on the surface with a slightly oblique incidence angle. Indeed, a deviation from the normal axis may favor the surface wave generation rate on one side of the slit. Another possibility is that the Au walls inside the slit may also be slightly asymmetric because of the ion beam etching treatment during the fabrication process. Finally, it is also possible that the fluorescent particle morphology break the symmetry.

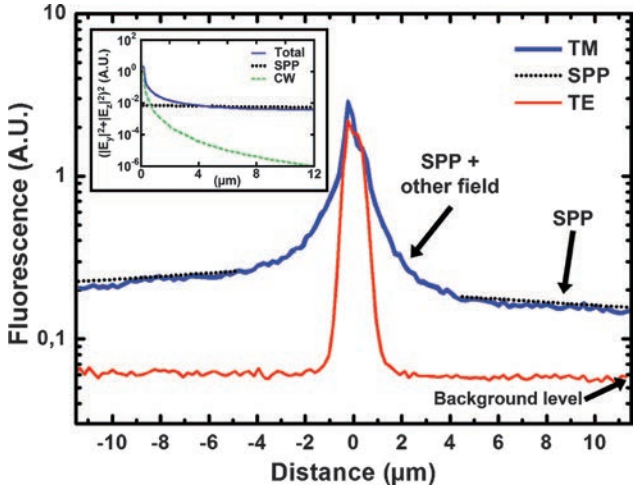

Fig. 3. (Color online) Near-field fluorescence data as a function of the slit distance extracted from the TE and TM images of Fig. 2. The data were obtained by averaging all the column data in the images of Fig. 2. The dotted curve represents the theoretical decay of the squared intensity of a SPP on gold. The inset represents computational data obtained under TM polarization, for the total field, the SPP contribution, and the CW contribution. The calculation is performed at 50 nm above the metal surface.

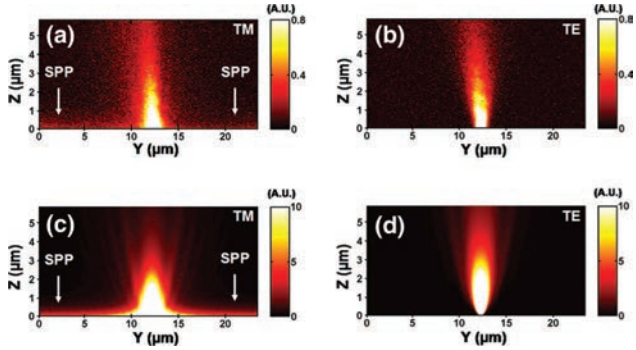

Fig. 4. (Color online) Near-field optical images in a plane perpendicular to the surface for TM and TE polarizations: (a), (b) experimental data; (c), (d) computational results. The images are slightly intensity saturated to show the presence of surface waves.

Nevertheless, despite the apparent asymmetry, the damping of the electromagnetic field essentially exhibits the same shape on both sides when moving away from the slit center. It is characterized by two regimes; a rapid decrease at small distances (< 3 μm) from the slit, followed by a slow decay at larger distances. The slow decay is almost perfectly exponential and fairly matches the theoretical decay of an SPP mode propagating at the gold–air interface [20]. The latter is represented by the dotted curves in Fig. 3. The curves, which are arbitrarily positioned in the vertical direction to fit the experimental data, scale as $\exp[-4\ \mathrm{Im}(k_{sp})x]$, where the fourth power stands for the nonlinear nature of the fluorescence measurements. We note that the experimental damping is slightly more pronounced than the theoretical one, probably because the gold layer is polycrystalline and presents some roughness. In the vicinity of the slit, the fluorescence data decrease at a much faster rate. The associated field contribution does not present any SPP character. According to previous works [4,9], it is formed by a quasi-cylindrical wave (CW) that creeps along the interface over distances of several wavelengths. This wave possesses a free-space character, with an amplitude scaling approximately as $1/\sqrt{x}\ \exp(ik_0x)$ [4,9,21].

To further analyze the experimental results, we have calculated the field diffracted 50 nm above the air–metal interface by the subwavelength slit with a full-vectorial aperiodic Fourier modal method (a-FMM) [22]. The fourth power of the predominant electric field component, $|\mathrm{E}|^4$, is shown by the solid curve in the inset of Fig. 3. The calculation has been performed for the same geometric parameters as those in the experiment and for a Au dielectric permittivity $\varepsilon_s = -44.1253 + 3.2507\,i$ [20]. From the total field, we have extracted the SPP contribution using the theoretical formalism in [19], and by difference the CW contribution (dotted curve). Consistent with the fluorescence experimental data, it is shown that the CW contribution decreases much faster than the SPP contribution, and that it is dominant at slit distances smaller than two wavelengths. All these experimental and computational data provide a direct confirmation of recent observations obtained with interference patterns produced with slit doublets [4].

All the previous results are related to the field scattered on the interface. For applications in nanophotonics, it is also interesting to know the radiation diagram above the slit in the near field. To answer this question, we performed noncontact scans in a plane perpendicular to the surface with the same tip. The corresponding SNOM images (slightly intensity-saturated to better reveal the surface waves) are represented in Figs. 4(a) and 4(b). Again, the SPP is clearly visible on the surface for TM polarization and absent for the TE case. We compared the experimental measurements with computational results. The latter that correspond to $|\mathrm{E}|^4$ are represented in Figs. 4(c) and 4(d). The overall resemblance is stringent: the same divergence pattern for TE and TM polarizations, the same surface waves and electromagnetic cloud around the slit for TM, and the absence of them for TE. The only difference is that the experimental data exhibit an asymmetry with respect to the direction normal to the interface. We do not know the exact cause of this observation, but the reasons discussed in relation with Fig. 3 are plausible. Additionally, we note that such asymmetry has previously been observed in far-field measurements performed for a circular aperture at microwave frequencies [23]. A rapid glance at the two images indicates that at large distances above the slit (>3–4 μm), the divergence of light in free space is not very different for the two polarizations. To confirm this observation, we also plotted the angular dependence of the measured scattered field in Fig. 5. The curves represent the signal intensity on a circle sit-

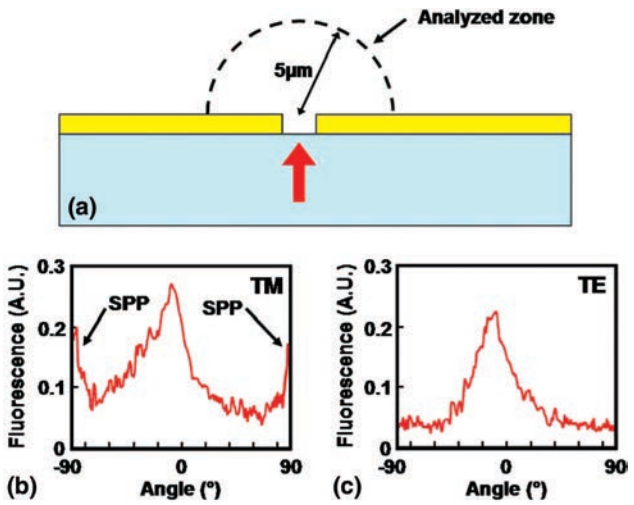

Fig. 5. (Color online) Experimentally measured signal on a circle of radius r = 5 μm from the slit center (a) analyzed zone. (b) Experimental data for TM polarization. (c) Same for TE. The curves are extracted from the experimental images in Fig. 4.

uated at 5 μm above the slit center. Apart from the presence of SPP waves for the TM polarization (located at directions −90° and +90°), the measured signals are similar. Another interesting characteristic of the TM curve is that at 5 μm from the slit center the SPP wave has an intensity comparable to the light diffracted at normal incidence, indicating that a large amount of energy is converted into an SPP and is not transmitted in the far field [19].

In summary, we have studied the electromagnetic field distribution near an isolated nanoslit aperture in a thin gold film using a fluorescent SNOM technique. We have clearly observed the two different contributions to the surface waves generated by the aperture on the interface under TM illumination. The measured field distribution is in good agreement with theoretical results. The observation of the surface waves in a lonely manner, without any interference, permits us to directly appreciate the SPP propagation on the surface and to evaluate its importance compared to the light diffracted in the far-field. This opens the way to characterize more complex structures, such as slit ensembles, and, for instance, to quantify the initial influence of SPPs or CWs to collimation effects resulting from the scattering by adjacent nanostructures.

The financial support of the Conseil Général de l'Essonne through the use of the equipment of the Centrale de Technologie Universtaire IEF-MINERVE is acknowledged. P. Lalanne and H. Liu thank Jean-Paul Hugonin for the fruitful discussions and computational assistance.

References

1. L. Yin, V. K. Vlasko-Vlasov, A. Rydh, J. Pearson, U. Welp, S.-H. Chang, S. K. Gray, G. C. Schatz, D. B. Brown, and W. C. Kinball, "Surface plasmons at single nanoholes in Au films," Appl. Phys. Lett. **85,** 467–469 (2004).
2. Z. Liu, J. M. Steele, W. Srituravanich, Y. Pikus, C. Sun, and X. Zhang, "Focusing surface plasmons with a plasmonic lens," Nano. Lett. **5,** 1726–1729 (2005).
3. H. Gao, J. Henzie, and T. W. Odom, "Direct evidence for surface plasmon-mediated enhanced light transmission through metallic nanohole arrays," Nano. Lett. **6,** 2104–2108 (2006).
4. L. Aigouy, P. Lalanne, J. P. Hugonin, G. Julié, V. Mathet, and M. Mortier, "Near-field analysis of surface waves launched at nanoslit apertures," Phys. Rev. Lett. **98,** 153902 (2007).
5. G. Gay, B. V. de Lesegno, R. Mathevet, J. Weiner, H. J. Lezec, and T. W. Ebbesen, "Atomic fluorescence mapping of optical field intensity profiles issuing from nanostructured slits milled into subwavelength metallic layers," Appl. Phys. B **81,** 871–874 (2005).
6. T. W. Ebbesen, H. J. Lezec, H. F. Ghaemi, T. Thio, and P. A. Wolff, "Extraordinary optical transmission through sub-wavelength hole arrays," Nature **391,** 667–669 (1998).
7. S. I. Bozhevolnyi, V. S. Volkov, E. Devaux, J. Y. Laluet, and T. W. Ebbesen, "Channel plasmon subwavelength waveguide components including interferometers and ring resonators," Nature **440,** 508–511 (2006).
8. K. A. Tetz, L. Pang, and Y. Fainman, "High-resolution surface plasmon resonance sensor based on linewidth-optimized nanohole array transmittance," Opt. Lett. **31,** 1528–1530 (2006).
9. P. Lalanne and J. P. Hugonin, "Interaction between optical nano-objects at metallo-dielectric interfaces," Nat. Phys. **2,** 551–556 (2006).
10. G. Gay, O. Alloschery, B. Viaris de Lesegno, J. Weiner, and H. J. Lezec, "Surface wave generation and propagation on metallic subwavelength structures measured by far-field interferometry," Phys. Rev. Lett. **96,** 213901 (2006).
11. F. Kalkum, G. Gay, O. Alloschery, J. Weiner, H. J. Lezec, Y. Xie, and M. Mansuripur, "Surface-wave interferometry on single subwavelength slit-groove structures fabricated on gold films," Opt. Express **15,** 2613–2621 (2007).
12. H. F. Schouten, N. Kuzmin, G. Dubois, T. D. Visser, G. Gbur, P. F. A. Alkemade, H. Blok, G. W.'t Hooft, D. Lenstra, and E. R. Elliel, "Plasmon-assisted two-slit transmission: Young's experiment revisited," Phys. Rev. Lett. **94,** 053901 (2005).
13. B. Hecht, B. Sick, U. Wild, V. Deckert, R. Zenobi, O. J. F. Martin, and D. W. Pohl, "Scanning near-field optical microscopy with aperture probes: fundamentals and applications," J. Chem. Phys. **112,** 7761–7774 (2000).
14. A. Bouhelier, T. Huser, H. Tamaru, H.-J. Güntherodt, D. W. Pohl, F. I. Baida, and D. Van Labeke, "Plasmon optics of structured silver films," Phys. Rev. B **63,** 155404 (2001).
15. J. C. Weeber, J. R. Krenn, A. Dereux, B. Lamprecht, Y. Lacroute, and J. P. Goudonnet, "Near-field observation of surface plasmon polariton propagation on thin metal stripes," Phys. Rev. B **64,** 045411 (2001).
16. L. Aigouy, Y. De Wilde, and M. Mortier, "Local optical imaging of nanoholes using a single fluorescent rare-earth-doped glass particle as a probe," Appl. Phys. Lett. **83,** 147–149 (2003).
17. H. Ditlbacher, J. R. Krenn, N. Felidj, B. Lamprecht, G. Schider, M. Salerno, A. Leitner, and F. R. Aussenegg, "Fluorescence imaging of surface plasmon fields," Appl. Phys. Lett. **80,** 404–406 (2002).
18. E. Verhagen, A. L. Tchebotareva, and A. Polman, "Erbium luminescence imaging of infrared surface plasmon polaritons," Appl. Phys. Lett. **88,** 121121 (2006).
19. P. Lalanne, J. P. Hugonin, and J. C. Rodier, "Approximate model for surface-plasmon generation at slit apertures," J. Opt. Soc. Am. A **23,** 1608–1615 (2006).
20. The gold permittivity is extracted from the tabulated data

in E. D. Palik, *Handbook of Optical Constants of Solids* (Academic Press, 1985), Part II(1).
21. L. Chen, J. T. Robinson, and M. Lipson, "Role of radiation and surface plasmon polaritons in the optical interactions between a nano-slit and a nano-groove on a metal surface," Opt. Express **14,** 12629–12636 (2006).
22. E. Silberstein, P. Lalanne, J. P. Hugonin, and Q. Cao, "Use of grating theories in integrated optics," J. Opt. Soc. Am. A **18,** 2865–2875 (2001).
23. M. J. Lockyear, A. P. Hibbins, J. R. Sambles, and C. R. Lawrence, "Surface-topography-induced enhanced transmission and directivity of microwave radiation through a subwavelength circular metal aperture," Appl. Phys. Lett. **84,** 2040–2042 (2004).